Supplementary Information for Electrical switching of spin-polarized light-emitting diodes based on a 2D CrI₃/hBN/WSe₂ heterostructure

Jianchen Dang[1], Tongyao Wu[1], Shuohua Yan[2,3], Kenji Watanabe[4], Takashi Taniguchi[5], Hechang Lei[2,3], Xiao-Xiao Zhang[1*]

[1]*Department of Physics, University of Florida, Gainesville, FL, United States*

[2]*Department of Physics and Beijing Key Laboratory of Opto-electronic Functional Materials & Micro-nano Devices, Renmin University of China, Beijing 100872, China*

[3]*Key Laboratory of Quantum State Construction and Manipulation (Ministry of Education), Renmin University of China, Beijing 100872, China*

[4]*Research Center for Functional Materials, National Institute for Materials Science, 1-1 Namiki, Tsukuba, Japan*

[5]*International Center for Materials Nanoarchitectonics, National Institute for Materials Science, 1-1 Namiki, Tsukuba, Japan*

Corresponding Author: xxzhang@ufl.edu
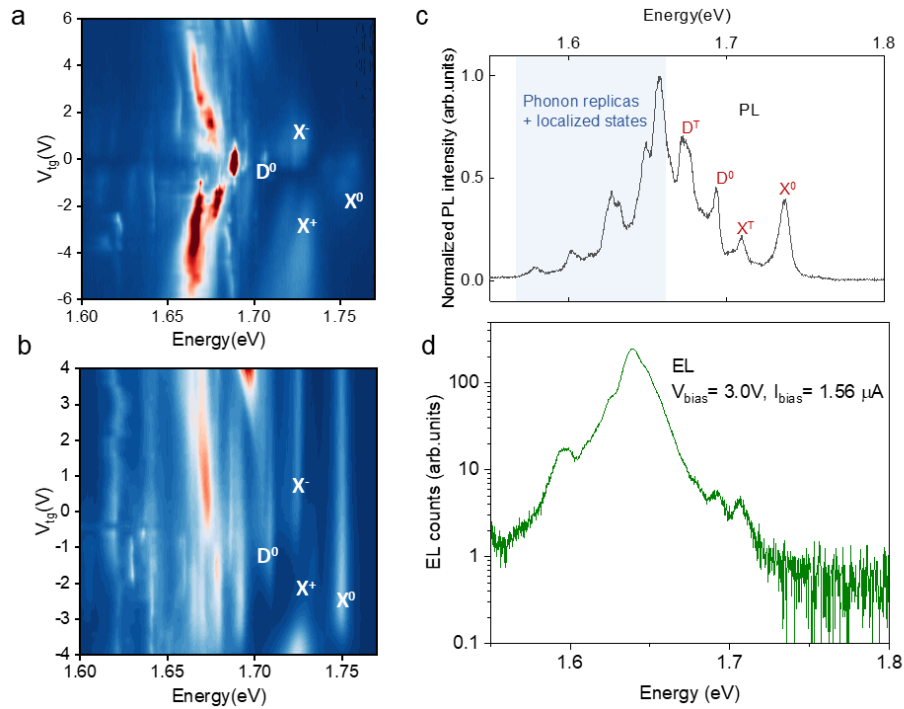
Supplementary Figures
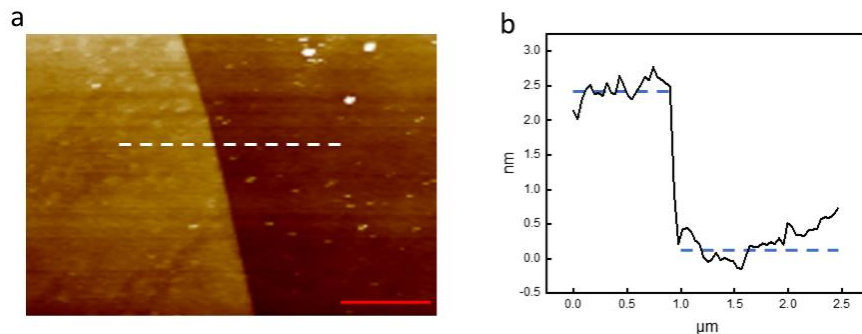
Supplementary Figure 1 AFM characterization of hBN barrier thickness for one of the devices.

(a) The atomic force microscope (AFM) image of an hBN barrier is presented. The dashed white line depicts a line cut of the step height differences. The red line represents a scale bar of 1μm. (b) The thickness profile line indicates a thickness of approximately 2.5 nm. Across all our devices, the hBN barrier thickness is consistently below 3 nm, identified by their color contrast under an optical microscope.
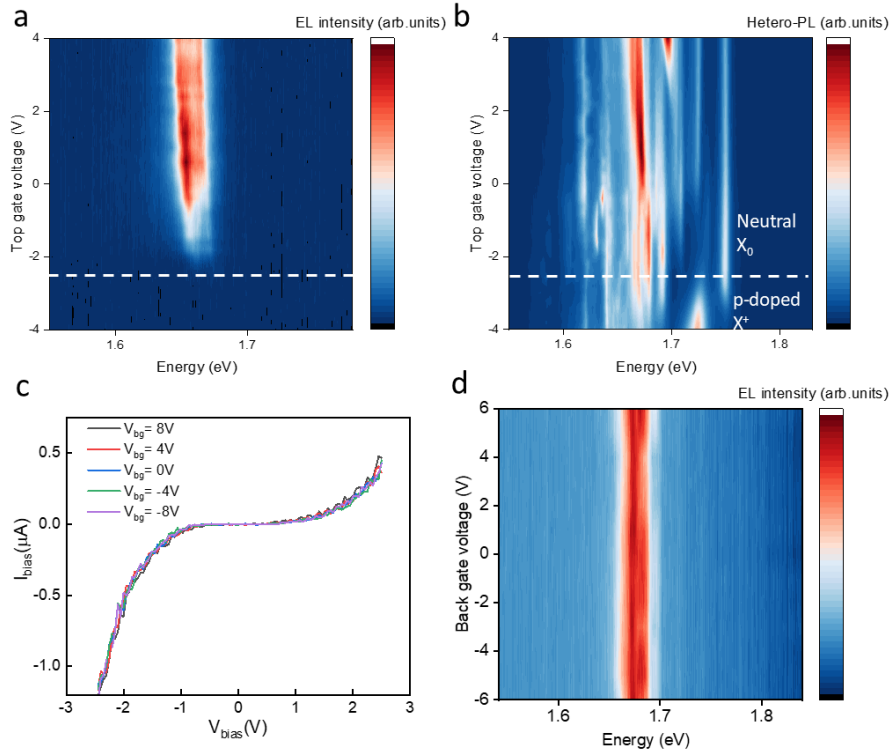
Supplementary Figure 2 Gate-dependent PL and EL of the devices.

(a) Top gate dependent EL measured at Vbias=2.5V. (b) Top gate dependent PL was measured in the heterostructure region at Vbias= 2.5V. For PL measurement, it is excited with 633nm continuous wave laser at 4K. The white dashed line indicates the onset of p-doping from the PL signals. The same doping also corresponds to the onset of the EL signals. (c) I_{bias}–V_{bias} characteristics at different back gate voltage when $V_{tg} = 0V$ for one of the bilayer CrI_3 devices. (d) Back gate dependent EL measured at $V_{bias} = 3.1V$ and $V_{tg} = 0V$. (c) and (d) indicate that the back gate has almost no effect on the bias current and EL intensity. This is expected and can be understood considering the large density of states (flat bands) of the CrI_3 band edges. With the finite electrostatic doping tuning capability, the corresponding Fermi level shifts in CrI_3 are much smaller than that can be achieved in WSe_2 and, therefore, do not have a significant impact on the I-V and EL intensity.
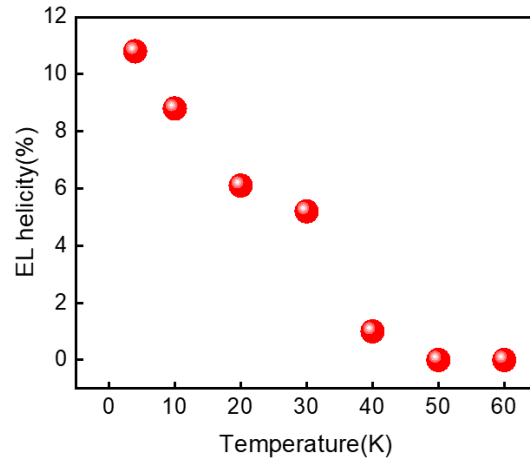
Supplementary Figure 3 Gate-dependent PL and comparison to EL spectrum.

(a) The top gate dependent PL of the region of monolayer WSe_2 in a device. The charge neutral point is located near 0V, as can be identified from the neutral bright (X^0) and dark exciton (D^0) near 0V, and from the emergence of positive trion (X^+) and negative trion (X^-) states when varying the V_{tg}. (b) The top gate dependent PL of the region of WSe_2/hBN/CrI_3 of the same device as in (a), which is the same as Supplementary Figure 2(b). The notation for exciton assigned is the same as in (a). Compared to (a), the neutral point is shifted down to ~ -3V. (c) A detailed assignment of exciton species for PL spectra is shown in the main text in Fig. 1f inset. X^T and D^T correspond to bright and dark trion states, and the exciton states were assigned based on the energy splitting between the lower energy exciton peaks and the bright neutral exciton. Due to the unintentional strain during sample fabrication, the peaks in the shaded area (localized states + phonon replicas) are merged and difficult to identify individually. (d) An EL spectrum plotted on a log scale in intensity. Excitonic states in EL spectra are most likely to originate from charged exciton states compared with the PL spectrum.
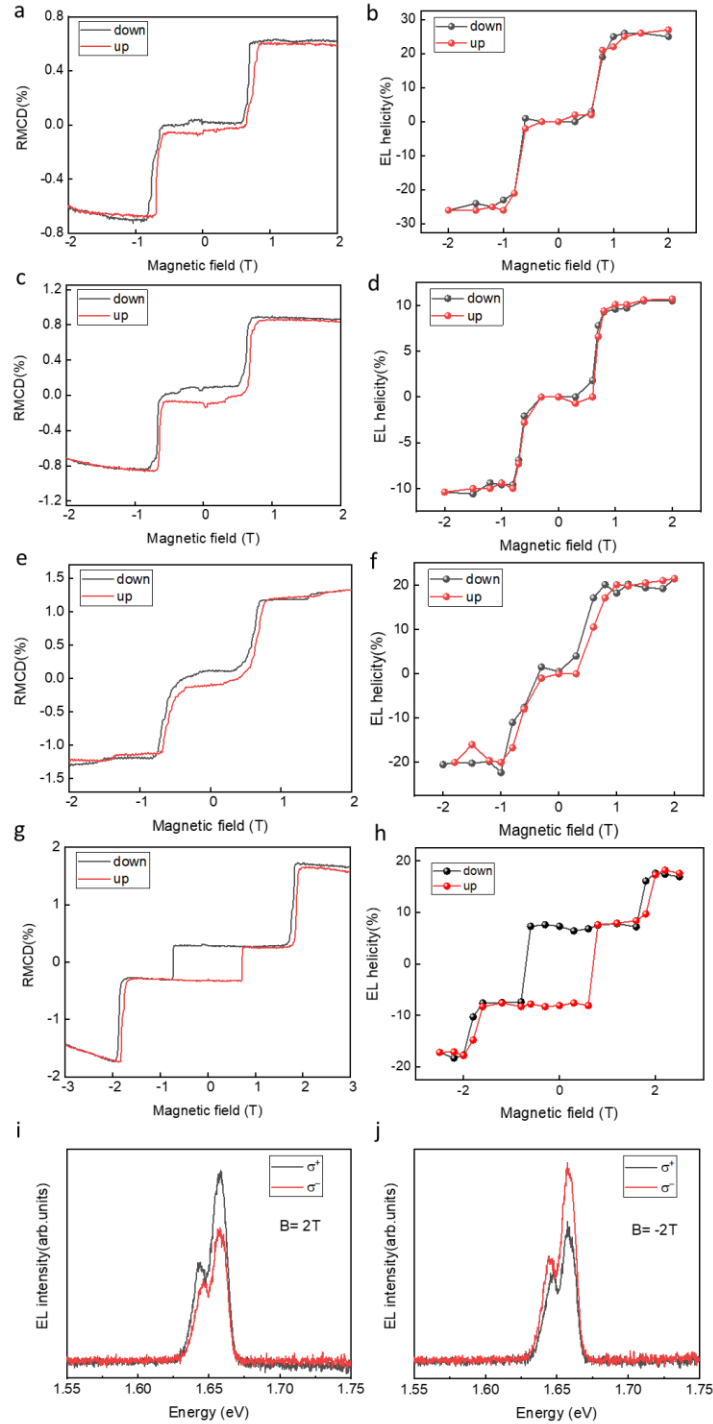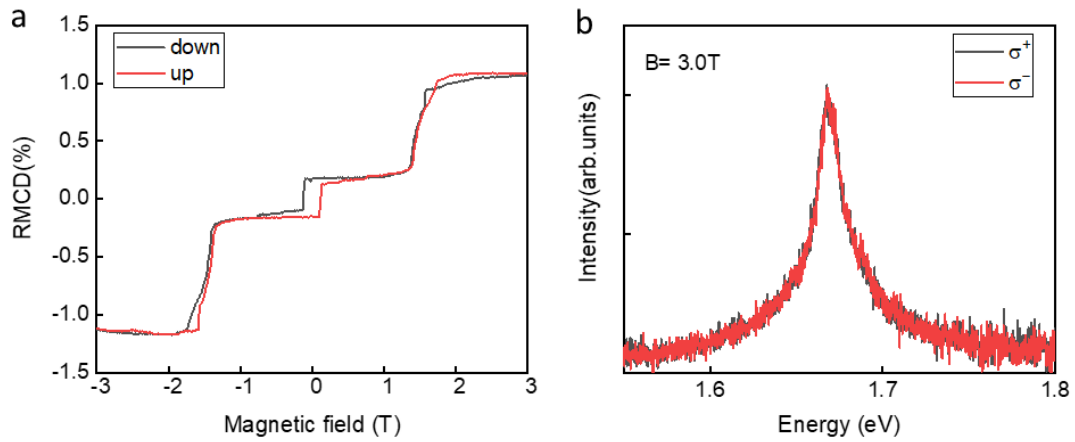
Supplementary Figure 4 Magnetic field dependences for additional bilayer and trilayer CrI₃ devices.

(a, c, e, g) RMCD signals and (b, d, f, h) corresponding EL helicity as a function of magnetic fields for bilayer and trilayer CrI₃ devices. (i) and (j) Polarization-resolved EL spectra under ±2T magnetic fields for the additional trilayer CrI₃ device (g and h), also showing opposite helicity.

Supplementary Figure 5 Temperature-dependent EL helicity.

The EL helicity decreases with increasing temperature and almost disappears for T ≥ 50 K, while the Neel temperature of the bilayer CrI_3 is approximately 45 K. This decrease can be attributed to two factors: the reduction in the magnetization of CrI_3 with temperature and the increase in phonon-assisted intervalley scattering as the temperature rises.
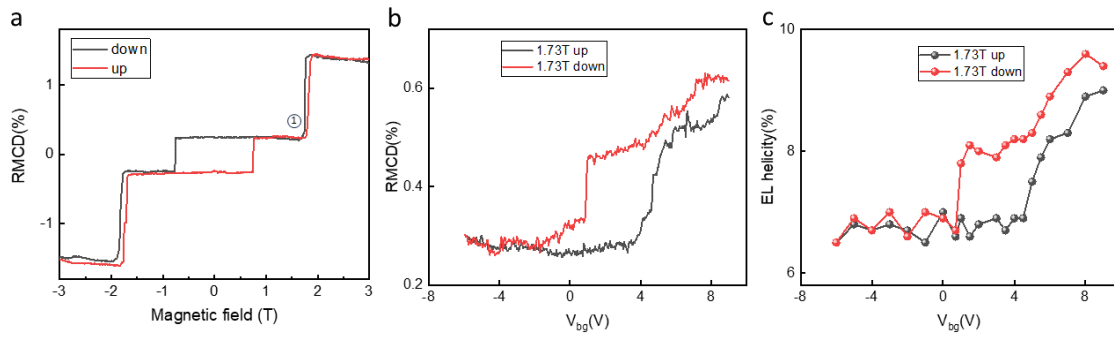
Supplementary Figure 6 EL helicity measurement on a device with no thin hBN tunneling barrier.

(a) RMCD signal is shown as a function of magnetic fields for this device. The result indicates that the CrI_3 in this device is a trilayer. (b) Polarization-resolved EL spectra under a 3T magnetic field. No noticeable difference in EL intensity was observed between σ^+ polarized and σ^- polarized detection.
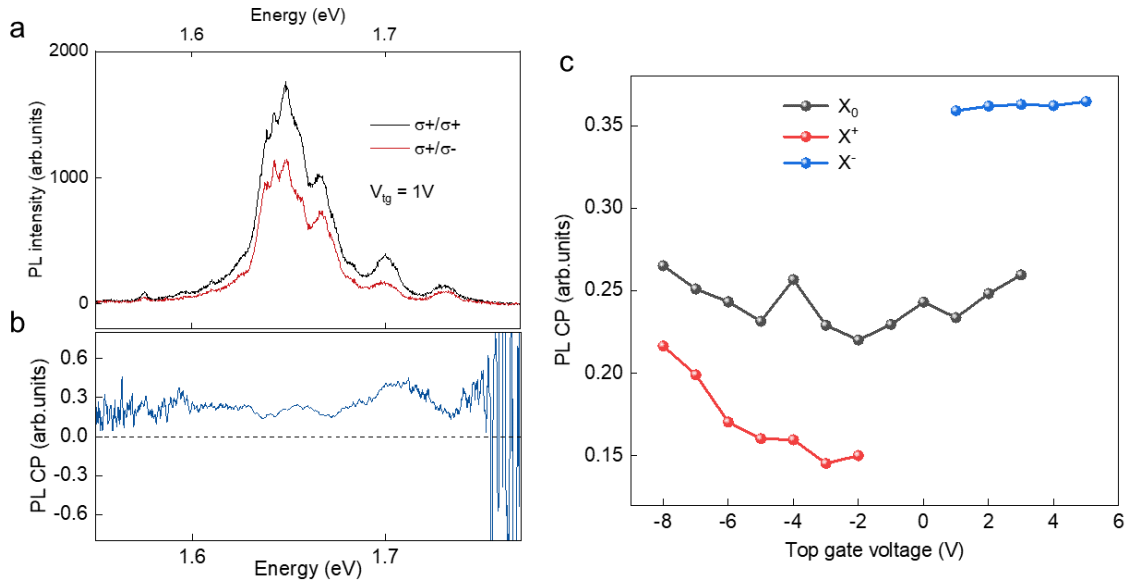
Supplementary Figure 7 Circular polarization measurements in monolayer WSe₂ PL.

(a) Polarization-resolved PL spectra under σ⁺ excitation with detection by σ⁺ and σ⁻ polarization. (b) The extracted degree of circular polarization as a function of energy from (a). (c) The top gate dependent circular polarization measurement for trions and neutral excitons in monolayer WSe₂. The measurement was conducted at 4K with 0T using a near-resonant 633nm continuous wave laser excitation. In the deeply doped region, for charge excitons, especially X⁻ excitons, the valley polarization $(I_{\sigma+} - I_{\sigma-})/(I_{\sigma+} + I_{\sigma-})$ is about 37%.

Supplementary Figure 8 Electrical switching of EL helicity for one of trilayer CrI₃ devices.

(a) RMCD of the trilayer CrI$_3$ as a function of the magnetic fields. (b) Back gate voltage control of RMCD of trilayer CrI$_3$ at a fixed magnetic field (1.73T). The sample was prepared by a magnetic field at 2T and then biased at 1.73T. (c) Corresponding EL helicity as a function of back gate voltages at a fixed 1.73T (trace 1 position).

Bilayer Devices	Saturation EL polarization (after SF)	
D1	10%	
D2	26%	
D3	10%	
D4	20%	
Trilayer Devices	**After first SF**	**After second SF**
D5	20%	40%
D6	8%	18%
D7	6%	NA

Supplementary Table 1 Saturation EL polarization among different devices.

The table summarizes the saturated EL polarization after the spin-flip (SF) transition for four bilayer CrI_3 devices and the polarization after the first SF and the second SF for three trilayer CrI_3 devices. For one of the trilayer CrI_3 devices (D7), the EL helicity above the second spin-flip transition was not measured because the device broke down.

Supplementary Note: Saturation EL polarization

To understand whether there is an evident correlation between the saturated EL polarization and the CrI_3 layer number, we measured magnetic field dependences of multiple bilayer and trilayer CrI_3 devices. It's worth noting that the EL helicity shows variation among different devices, possibly attributed to differences in device quality. The saturation polarization for EL among different devices is shown in Supplementary Table 1.